MARINET

Marine Renewables Infrastructure Network

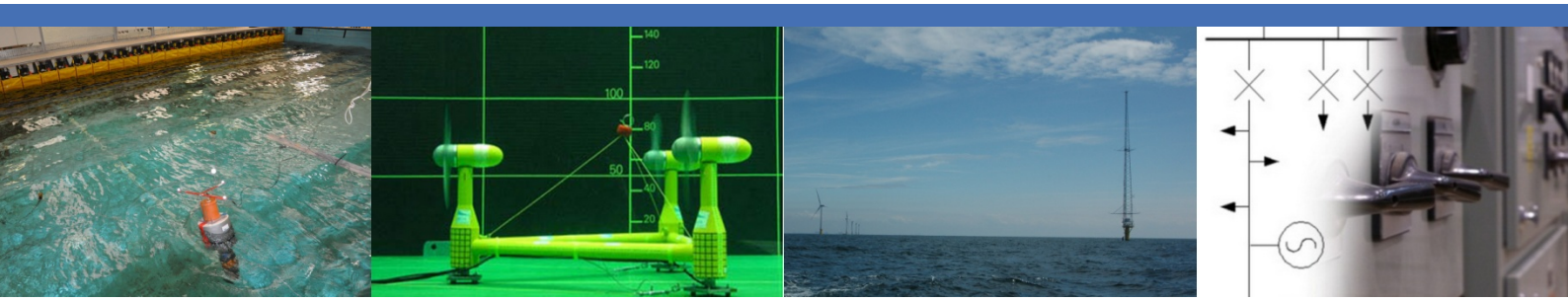

WP4: Research to Innovate and Improve Infrastructures, Technologies and Techniques

Deliverable D4.04EC

Report on low frequency response and moorings

Status:	Final
Version:	02
Date:	05-May-2014

SEVENTH FRAMEWORK PROGRAMME

ABOUT MARINET

MARINET (Marine Renewables Infrastructure Network for emerging Energy Technologies) is an EC-funded network of research centres and organisations that are working together to accelerate the development of marine renewable energy - wave, tidal & offshore-wind. The initiative is funded through the EC's Seventh Framework Programme (FP7) and runs for four years until 2015. The network of 29 partners with 42 specialist marine research facilities is spread across 11 EU countries and 1 International Cooperation Partner Country (Brazil).

MARINET offers periods of free-of-charge access to test facilities at a range of world-class research centres. Companies and research groups can avail of this Transnational Access (TA) to test devices at any scale in areas such as wave energy, tidal energy, offshore-wind energy and environmental data or to conduct tests on cross-cutting areas such as power take-off systems, grid integration, materials or moorings. In total, over 700 weeks of access is available to an estimated 300 projects and 800 external users, with at least four calls for access applications over the 4-year initiative.

MARINET partners are also working to implement common standards for testing in order to streamline the development process, conducting research to improve testing capabilities across the network, providing training at various facilities in the network in order to enhance personnel expertise and organising industry networking events in order to facilitate partnerships and knowledge exchange.

The initiative consists of five main Work Package focus areas: Management & Administration, Standardisation & Best Practice, Transnational Access & Networking, Research, Training & Dissemination. The aim is to streamline the capabilities of test infrastructures in order to enhance their impact and accelerate the commercialisation of marine renewable energy. See www.fp7-marinet.eu for more details.

Partners

Ireland
University College Cork, HMRC (UCC_HMRC) *Coordinator*
Sustainable Energy Authority of Ireland (SEAI_OEDU)

Denmark
Aalborg Universitet (AAU)
Danmarks Tekniske Universitet (RISOE)

France
Ecole Centrale de Nantes (ECN)
Institut Français de Recherche Pour l'Exploitation de la Mer (IFREMER)

United Kingdom
National Renewable Energy Centre Ltd. (NAREC)
The University of Exeter (UNEXE)
European Marine Energy Centre Ltd. (EMEC)
University of Strathclyde (UNI_STRATH)
The University of Edinburgh (UEDIN)
Queen's University Belfast (QUB)
Plymouth University(PU)

Spain
Ente Vasco de la Energía (EVE)
Tecnalia Research & Innovation Foundation (TECNALIA)

Belgium
1-Tech (1_TECH)

Netherlands
Stichting Tidal Testing Centre (TTC)
Stichting Energieonderzoek Centrum Nederland (ECNeth)

Germany
Fraunhofer-Gesellschaft Zur Foerderung Der Angewandten Forschung E.V (Fh_IWES)
Gottfried Wilhelm Leibniz Universität Hannover (LUH)
Universitaet Stuttgart (USTUTT)

Portugal
Wave Energy Centre – Centro de Energia das Ondas (WavEC)

Italy
Università degli Studi di Firenze (UNIFI-CRIACIV)
Università degli Studi di Firenze (UNIFI-PIN)
Università degli Studi della Tuscia (UNI_TUS)
Consiglio Nazionale delle Ricerche (CNR-INSEAN)

Brazil
Instituto de Pesquisas Tecnológicas do Estado de São Paulo S.A. (IPT)

Norway
Sintef Energi AS (SINTEF)
Norges Teknisk-Naturvitenskapelige Universitet (NTNU)

DOCUMENT INFORMATION

Title	Report on low frequency response and moorings
Distribution	[Choose distribution authorisation]
Document Reference	MARINET-D4.04
Deliverable Leader	Marc Le Boulluec Ifremer
Contributing Authors	Marc Le Boulluec Ifremer

REVISION HISTORY

Rev.	Date	Description	Prepared by (Name & Org.)	Approved By (Task/Work-Package Leader)	Status (Draft/Final)
01	08-Apr-2014	Draft	Marc Le Boulluec Ifremer		Draft
02	05-May-2014	Revision according to remarks from WPL	Marc Le Boulluec Ifremer	Jochen Giebhardt IWES Lars Johannig UNIEXE	Final

ACKNOWLEDGEMENT

The work described in this publication has received support from the European Community - Research Infrastructure Action under the FP7 “Capacities” Specific Programme through grant agreement number 262552, MaRINET.

LEGAL DISCLAIMER

EXECUTIVE SUMMARY

Floating bodies experiencing the combined action of wind, waves and currents show a dynamic response with multiple frequencies motions. The basic formulation for sea keeping is based on the perfect fluid assumption. The development at first and second orders shows a theoretical linear response to the waves frequencies and a theoretical quadratic response at low frequencies and high frequencies.
The natural frequencies of the floating bodies depend on the type of mooring, usually natural frequencies of the vertical motions (heave, roll, pitch) are included in the wave frequency range and natural frequencies of the horizontal motions (surge, sway, yaw) are included in the low frequency range, but in some circumstances this behaviour may differ (tension legs, deep draft column).
The amplitude of the response around resonance depend on the damping ratio of the system. The perfect fluid assumption leads to linear wave frequency and low frequency drift damping, but additional non linear damping arise from the viscous real flow related to the floating bodies hulls and moorings.

As part of the European Interreg IV-A MERiFIC (Marine Energy in Far Peripheral and Island Communities) project, a collaborative work between Ifremer and the University of Exeter was conducted with a specific focus on the subject of synthetic mooring lines for MRE converters. The South Western Mooring Test Facility (SWMTF) is a moored buoy operated by the University of Exeter in the Falmouth Bay, UK. The purpose of this buoy is the assessment of moorings and in particular, synthetic mooring lines.
Tests of the buoy at a reduced 1/5 scale were conducted in the wave tank of Ifremer in Plouzané, France. Decay tests, regular wave tests and irregular wave tests were conducted. Different kind of mooring lines were tested: stiff lines, soft lines and lines with an increased diameter and roughness to represent marine growth (bio-fouling).
This case study illustrates the first and second order effects and the influence of the mooring lines on the surge drift response.

Two different frequency intervals are clearly visible from the tests results :
- one related to the incoming waves frequency
- one related to the low frequency response

In the wave frequency range, for a mooring lines configuration, the higher the significant waves height, the lower the RAO at resonance. This behaviour is typically related to the non linear damping of the heave and pitch motions.

In the low frequency range, the surge resonance amplitude depends on the mooring lines configuration and decrease when the mooring lines are fitted with nets simulating the marine growth which are increasing the damping effect.
It can be noted that the mean surge drift is increased in the case of the mooring lines with a larger diameter simulating the presence of bio-fouling. Wave effects on these large diameter lines can be important.

Addition of strong numerical damping to simulate the action of a possible power take-off (30% of heave or pitch critical damping) shows that the mean drift surge force may evolve considerably.
This phenomenon should be analysed through model testing as well as the approximation of the mooring lines damping at low frequency.

CONTENTS

1 INTRODUCTION

1.1 LOW FREQUENCY RESPONSE AND MOORINGS

Floating bodies experiencing the combined action of wind, waves and currents show a dynamic response with multiple frequencies motions. The basic formulation for sea keeping under the perfect fluid assumption when developed to the first and second orders in the particular case of waves [Lee 1991, Chen 2004, Chen 2009], shows a linear response to the waves frequencies and second order responses at low frequencies and high frequencies (figure 1.1 and figure 1.2). In the case of bi-chromatic waves or multi-chromatic waves the second order terms are related to cross products of first order terms giving rise to double, sum and difference frequencies (figure 1.2).

Usually, without mooring, the natural frequencies related to the vertical motions (heave, roll, pitch) are within the waves spectra frequency range, except for the particular case of deep draft floaters, such as SPAR, whose natural heave periods can be quite long compared to the incoming waves periods.
Depending on the type of mooring, the natural frequencies of a floating body may also evolve.

With soft catenary mooring lines, such as those used for semi-submersibles, the hydrostatics stiffness matrix is dominant and the natural frequencies related to the vertical motions remain in the waves frequency domain. The natural frequencies related to the horizontal motions (surge, sway, yaw) are generally low because of small mooring stiffness compared to the hydrostatics and large inertia. When bi-chromatic waves or multi-chromatic waves are considered (Figure 1.2), the difference frequency can be much smaller than the initial frequencies and be close to the natural frequencies of floating bodies anchored with soft moorings, so that low frequency resonance generally happens. The low frequency resonance may initiate large amplitude motions and induce high loads in the mooring lines. The interaction with other floating bodies is also influenced by the low frequency response and can lead to difficulties in the case of farms where devices are deployed in close vicinity or access with tender boats.
The low frequency motions response is the result of the action of the low frequency forces on the mass-spring-damping system which represents the floating body [Sarkar 1998, 2000, 2001]. As a resonant phenomenon, the low frequency response is limited by the low frequency damping.
This damping has several sources [Le Boulluec 1994] :

- the so-called wave drift damping induced by the variation of the mean drift forces when the floating body experiences slow forward velocity
- viscous damping which is related to the drag and friction effects on the buoy and on the mooring lines, this second type of viscous damping can be an important part of the total low frequency damping [Bompais 1994]

With vertical taught mooring lines, like for instance in the case of Tension Legs Platforms, the mooring stiffness can be dominant and the natural frequencies related to the vertical motions become higher than the waves frequencies.
With inclined taught mooring lines, all natural frequencies of the floating body may become higher than the waves frequencies. When bi-chromatic waves are considered (figure 1.2), the sum frequency can be close to these high natural frequencies possibly inducing high frequency resonance.

In the case of marine energy converters the mooring is an important issue [Retzler 2006], particularly in the case of wave energy converters when the mooring can be coupled of the power take off.

The purpose of this report is to illustrate the low frequency response of moored floating bodies in the context of marine energy devices. Hence a case study is presented and experimental results are compared to numerical data. Semi analytical methods developed for the evaluation the influence of the moorings on the slow drift damping are given in Appendices.

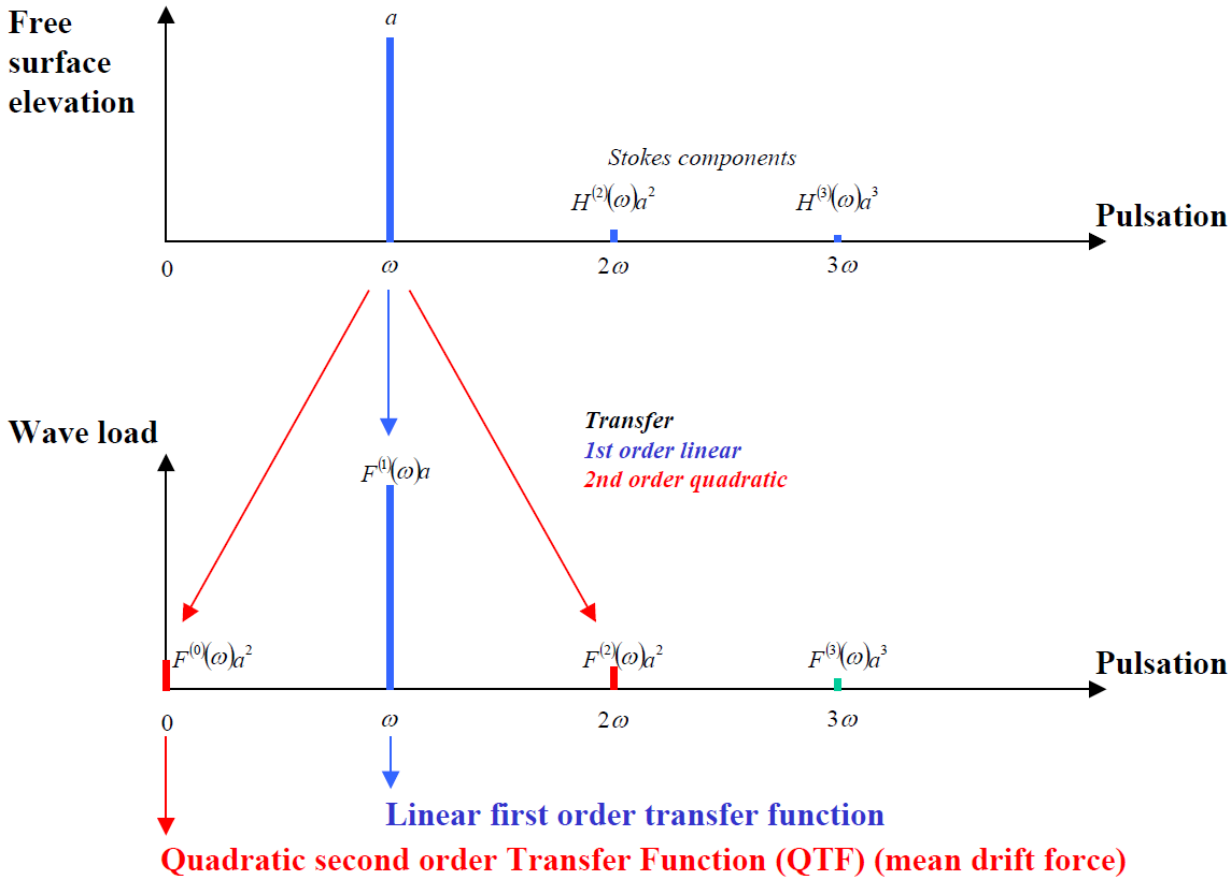

Figure 1.1 First and second order effects - Monochromatic waves

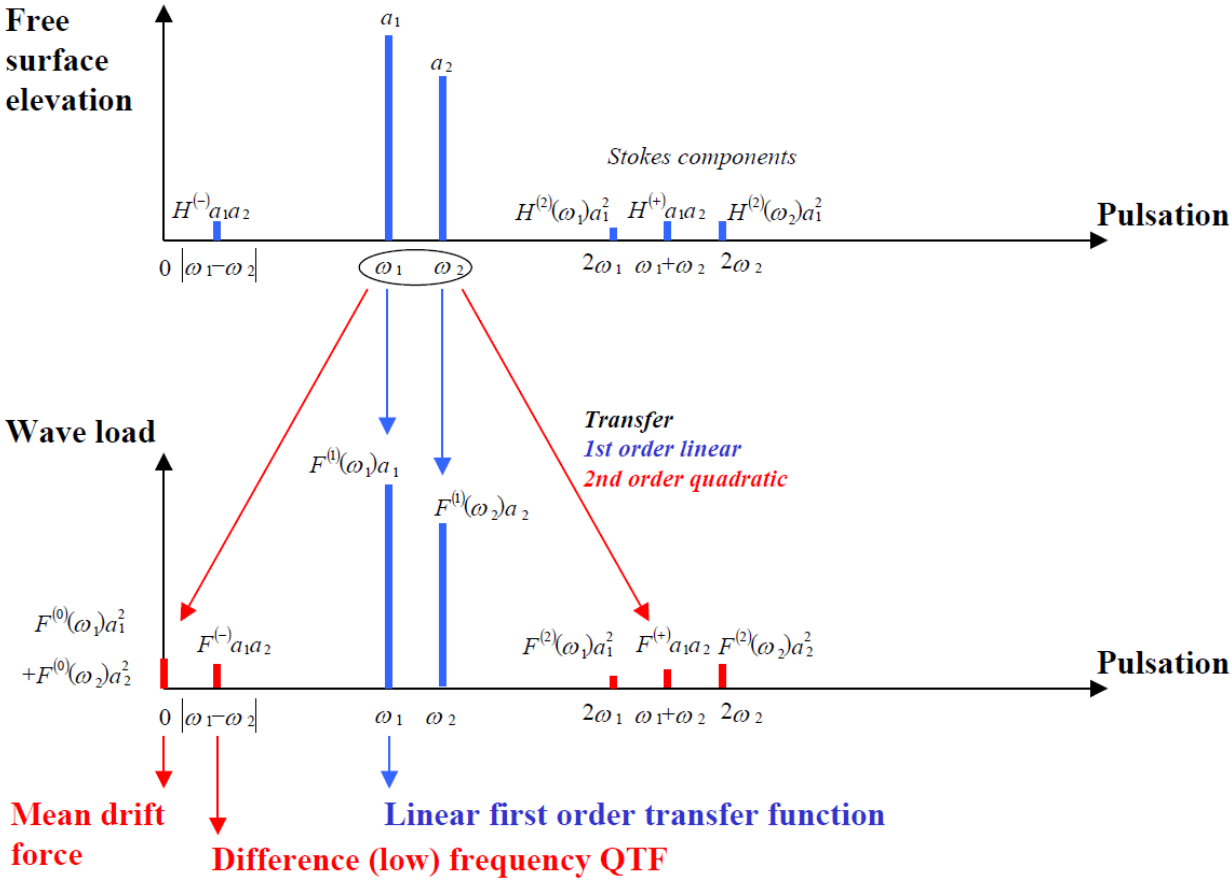

Figure 1.2 First and second order effects - Bi-chromatic waves

2 CASE STUDY

It was initially scheduled in the MARINET project to analyse tests done with a wave energy converter and describe its response, and particularly its low frequency response with and without power take off.
Because of lack of data it was finally decided to consider the case of a buoy without power take off.

As part of the European Interreg IV-A MERiFIC (Marine Energy in Far Peripheral and Island Communities) project, a collaborative work between Ifremer and the University of Exeter was conducted with a specific focus on the subject of synthetic mooring lines for MRE converters. The South Western Mooring Test Facility (SWMTF) is a moored buoy operated by the University of Exeter in the Falmouth Bay, UK (figure 2.1). The purpose of this buoy is the assessment of moorings and in particular, synthetic mooring lines [Weller 2013]. Three mooring lines, equipped with load celles, are spread at 120° angles. Two mooring lines are facing the main waves direction.

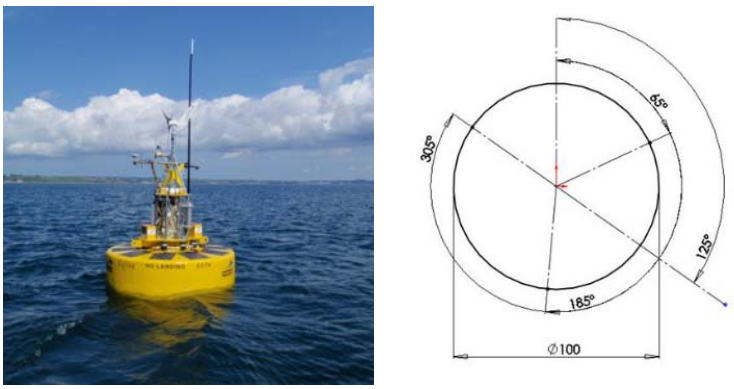

Figure 2.1 South Western Mooring Test Facility an Mooring layout – University of Exeter

Tests of the buoy at a reduced 1/5 scale were conducted in the wave tank of Ifremer in Plouzané, France (figure 2.2). Decay tests, regular wave tests and irregular wave tests were conducted. Different kind of mooring lines were tested: stiff lines, soft lines and lines with an increased diameter and roughness to represent marine growth (bio-fouling).
During these tests in the wave tank, the incoming waves, the buoy motions and the mooring line tensions were measured. These measurements enabled comparison with the results of different coupled numerical tools (diffraction and radiation including Quadratic Transfer Functions, mooring lines modelling).

In this report, the motions of the moored buoy in waves are studied, especially the low frequency surge behaviour.
According to figure 1.1, tests in regular waves give information on the mean drift forces or motions.
According to figure 1.2, tests in irregular waves give information on the mean drift forces or motions and on the low frequency response.

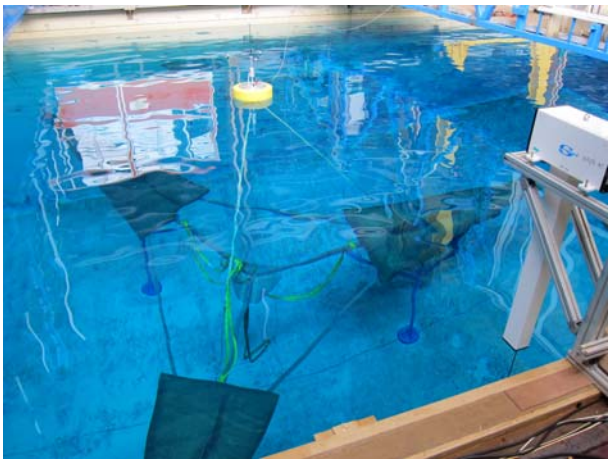

Figure 2.2 1/5 scaled buoy in the Ifremer wave tank

Different methods of analysis can be used to extract the second order components of the response [Jamsek 2003, Kim 2004, Sibetheros 2000].

In this study the mean surge drift motion of the buoy in regular and irregular waves as well as the low frequency energy part of the power density spectrum of the surge motion in irregular waves are analysed.

The mooring lines are combination of chains and textile ropes. During the model scale tests different textile ropes were tested : a stiff line, a soft line, a soft line with net figuring the bio-fouling growth (figure 2.3).

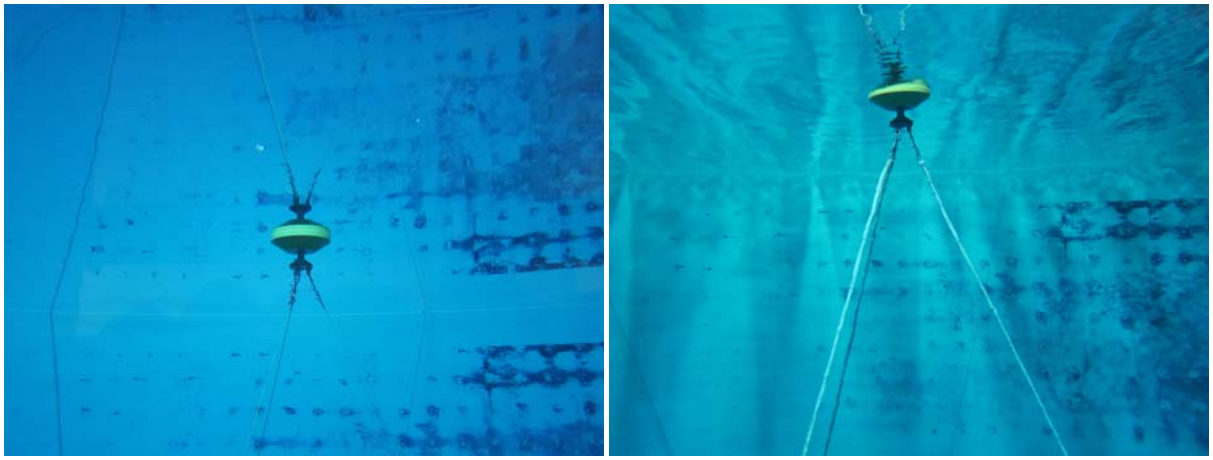

Figure 2.3 Underwater views of the buoy and its mooring lines at Ifremer wave tank.

Left: lines without bio-fouling. Right: lines with bio-fouling simulated by aggregated nets.

3 COMPARISON OF EXPERIMENTAL AND NUMERICAL RESULTS

Additionaly to the experimental assessment of the low frequency response of the buoy, a numerical study was conducted using a diffraction/radiation code so as to validate the results and provide some insight on the influence of viscosity effects and nonlinearities.

3.1 NUMERICAL SIMULATION

The numerical simulation of the buoy behaviour in waves were conducted using the diffraction and radiation software Hydrostar developed by Bureau Veritas [Chen 2009]. The results are the classical first order waves forces, added masses and linear damping and the second order difference frequency Quadratic Transfer Functions (QTF).
The QTF are computed considering bi-chromatic incoming waves and taking into account their interaction with the floating buoy (figure 1.2). The diagonal of the QTF corresponds to the zero difference frequency and consists of the mean drift force transfer function.
The mean drift surge motion is computed dividing the mean drift force by the mooring stiffness in the surge direction.
On regular waves, the evaluation of the mean drift surge motion is straightforward.
On irregular waves, the contribution of all components of the wave spectrum must be calculated.

$F_d(\omega)$	Mean drift force transfer function
$X_d(\omega)$	Mean surge drift transfer function on regular waves
X_{do}	Mean surge drift value on irregular waves
$S(\omega)$	Waves power density spectrum
T_p	Peak Period
H_s	Significant wave height
K_{xx}	Surge mooring stiffness

$$X_d(\omega)=\frac{F_d(\omega)}{K_{xx}} \qquad X_{do}=\frac{2}{K_{xx}}\int_0^\infty S(\omega)F_d(\omega)d\omega \qquad H_s=4\sqrt{\int_0^\infty S(\omega)d\omega}$$

In order to analyse the effects of a possible power take-off, additional damping was introduced in the numerical simulation : 30 % of the heave critical damping on one hand and 30% of the pitch critical damping on the other hand.

3.2 EXPERIMENTAL RESULTS

Comparisons are made with the data sets measured during the wave tank testing so that results hereafter are given at model scale (1/5). An example of the response of the buoy on irregular waves is shown on figures 3.1 and 3.2.

3.2.1 Incoming waves and lines tensions

Figure 3.1 depicts the power density spectrum of the incoming waves as measured by two gauges placed in the wave tank in the vicinity of the model and compared to the targeted JONSWAP spectrum (red thick line) together with the power density spectrum of the tensions measured in the three mooring lines.
Two different frequency intervals are clearly visible on the lines tension spectra :

- one related to the incoming waves frequency in the range [0.2, 2] Hz
- one related to the low frequency response in the range [0, 0.2] Hz.

3.2.2 Motions

Figure 3.2 depicts the power density spectrum of the motions. Even though the six degrees of freedom are presented here, it should be noted that in the configuration of the testing set-up where only unidirectional waves were consideredonly the surge, heave and pitch motions are relevant, whilst sway, roll and yaw motions are the result of a slight axial dissymmetry in the experimental setting.

Here again two different frequency intervals are clearly visible :

- one related to the incoming waves frequency in the range [0.2, 2] Hz
- one related to the low frequency response in the range [0, 0.2] Hz.

It is important to note that only the horizontal motions show low frequency components.

Two significant surge values can be assessed from these spectra : one for the waves frequency interval and one for the low frequency interval.

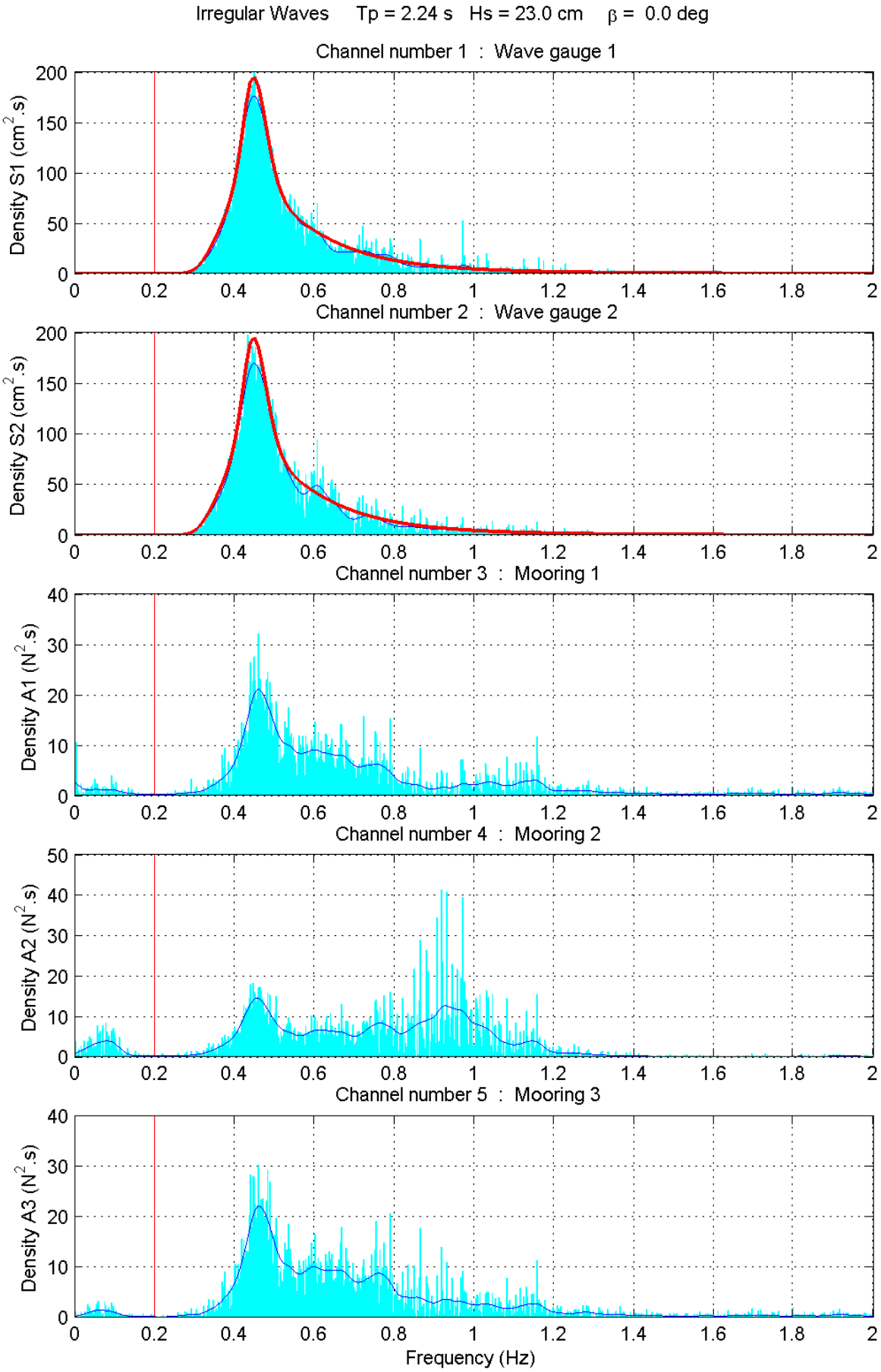

Figure 3.1 Irregular waves spectrum and mooring lines tensions

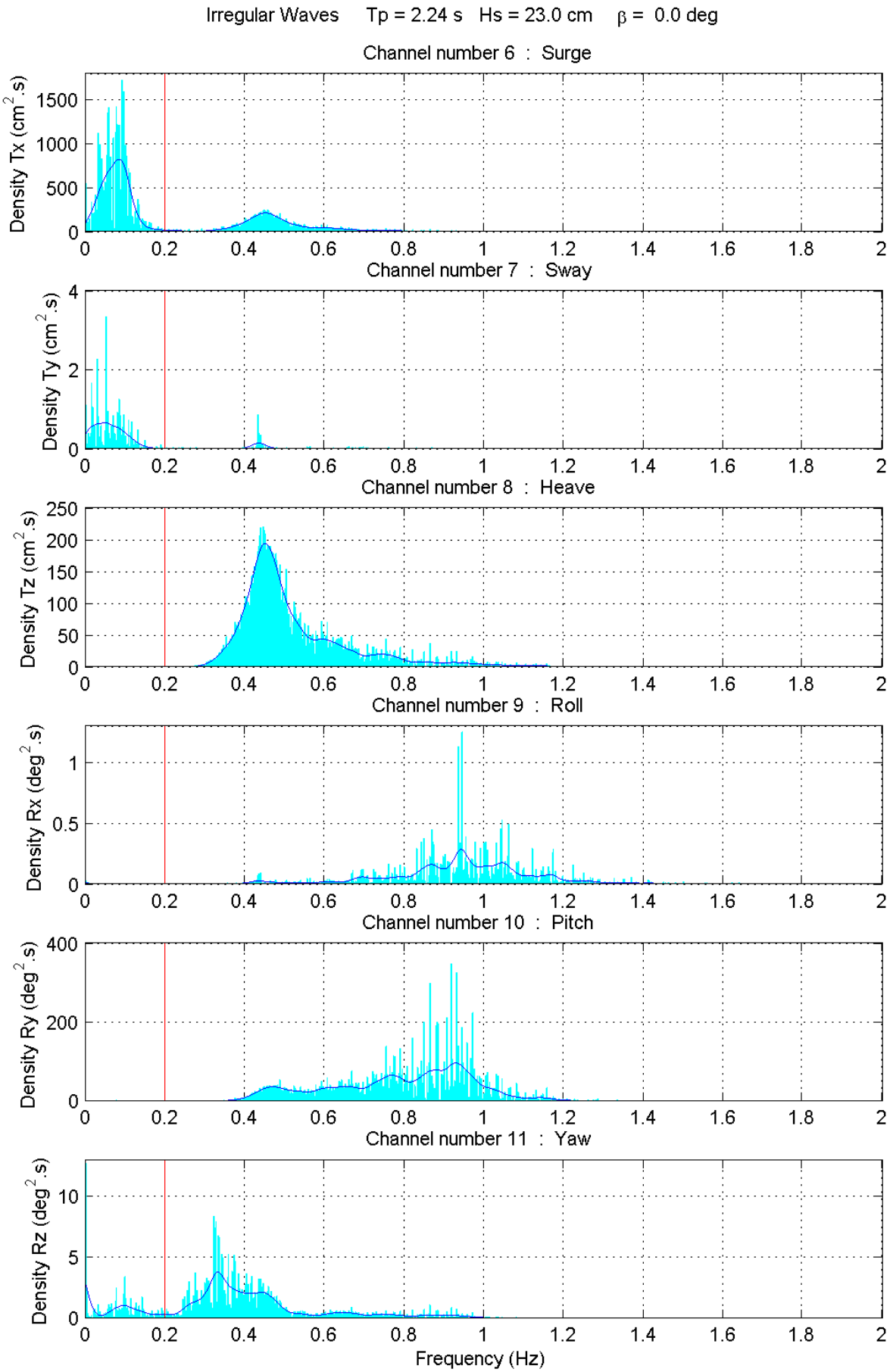

Figure 3.2 Motions spectrum on irregular waves

3.3 COMPARISON

Results are compared at model scale (1/5).

3.3.1 First order response on regular and irregular waves

Figure 3.3 (graphs 1 to 3 from the top) depicts the comparison between the numerical transfer functions and the experimental RAOs for surge, heave and pitch motions.

On these plots, the red thick line is the numerical transfer function to be compared to the experimental results. Markers are associated with the wave height of the various tests conducted in regular waves whilst colors of the lines are related to the type of rope used for the mooring.

Red thick line : numerical transfer function to compare to the experimental data.

Regular waves experiments : wave height H 3 5 8 10 20 30 40 50 cm
◇ ▽ □ △ ○ + × ✳
Blue marker : stiff rope
Red marker : soft rope
Green marker : soft rope with bio-fouling

Irregular waves experiments :
Blue line : stiff rope
Red line : soft rope
Green line : soft rope with bio-fouling

The comparison of the first order numerical results is satisfactory for the three motions.
Constant linear damping representing the viscous effects (heave : 3%, pitch : 7%) has been added to the linear wave damping to better fit the resonance of the vertical motions. Anyway the comparison shows that non linear additional damping should be added for a better simulation of the viscous effects which depend on the response level.

For a mooring lines configuration, the higher the significant waves height, the lower the RAO at resonance.

3.3.2 Mean surge drift on regular waves

Comparison between the numerical surge drift transfer function and the experimental results is presented on the bottom graph of the figure 3.3. On these plot, the colours of the thick lines corresponding to the numerical transfer functions are related to the various damping coefficients which were implemented:

Red thick line : numerical transfer function to compare to the experimental data.
Black thick line : numerical transfer function with additional 30% critical heave damping
Blue thick line : numerical transfer function with additional 30% critical pitch damping

Comparison between the numerical surge drift transfer function and the experimental results is quite good.
However, slight discrepancies appear on both side of the pitch resonance that could be corrected with a better evaluation of the heave and pitch viscous damping which depends on the wave period and wave height as well as on the response level.

It can be noted that the mean surge drift is increased in the case of the mooring lines with a larger diameter simulating the presence of bio-fouling (green markers). Wave effects on these large diameter lines can be important.

Addition of strong damping to simulate the action of a possible power take-off (30% of critical damping) shows that the mean drift surge force may evolve considerably.

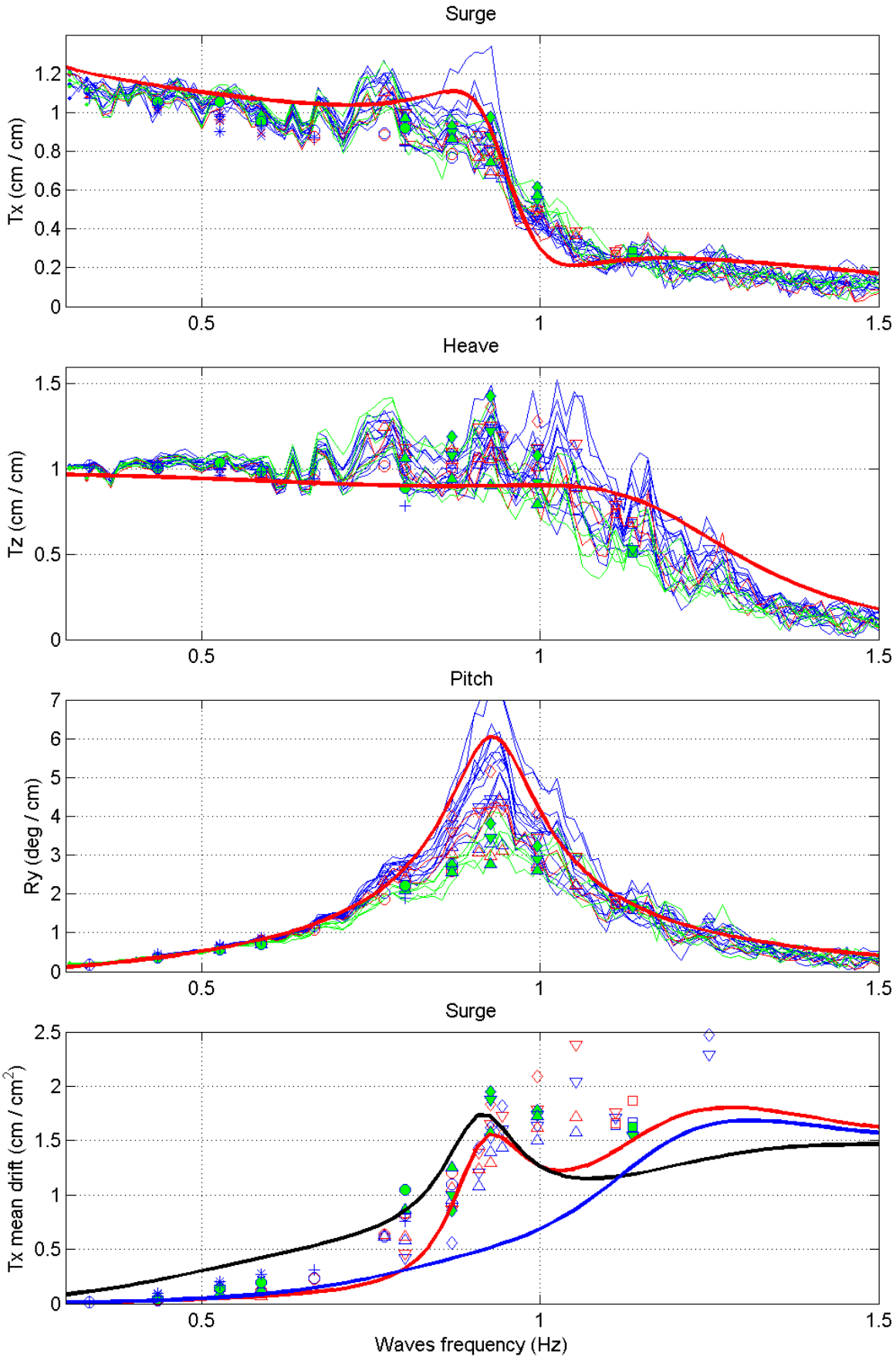

Figure 3.3 Waves frequency response on regular and irregular waves. Mean surge drift on regular waves.

3.3.3 Mean drift response on irregular waves

Figure 3.4 (top graph) depicts the comparison between the numerical transfer functions of the mean surge drift and the experimental RAO for surge.

Red thick line : numerical transfer function to be compared to the experimental data.

Irregular waves experiments : significant wave steepness s ▽ ○ △ □

$$s=2\pi\frac{H_s}{gT_p^2} \qquad s<1 \quad 1\le s<2 \quad 2\le s<3 \quad 3\le s<4$$

Blue marker : stiff rope
Red marker : soft rope
Green marker : soft rope with bio-fouling

The comparison of the second order numerical results is satisfactory.
The mean surge drift increases when the mooring lines are fitted with nets simulating the marine growth.
As stated in 3.3.1 for the regular waves case, the wave effects on the mooring lines with enlarged diameter may increase the mean drift.
For the shorter waves peak periods, the measured mean surge drift is lower than expected from the numerical results, because the mooring stiffness increases with the amplitude of the surge motion and the mean surge motion increases for the shorter peak periods.

3.3.4 Slow drift response on irregular waves

Figure 3.4 (bottom graph) depicts the experimental second order low frequency significant surge.

Irregular waves experiments : significant wave steepness s ▽ ○ △ □

$$2\pi\frac{H_s}{gT_p^2}=s \qquad s<1 \quad 1\le s<2 \quad 2\le s<3 \quad 3\le s<4$$

Blue marker : stiff rope
Red marker : soft rope
Green marker : soft rope with bio-fouling

The significant low frequency surge is higher for wave spectras with shorter peak period. It can also be noted that it decreases when the mooring lines are fitted with nets simulating the marine growth which are increasing the damping effect.

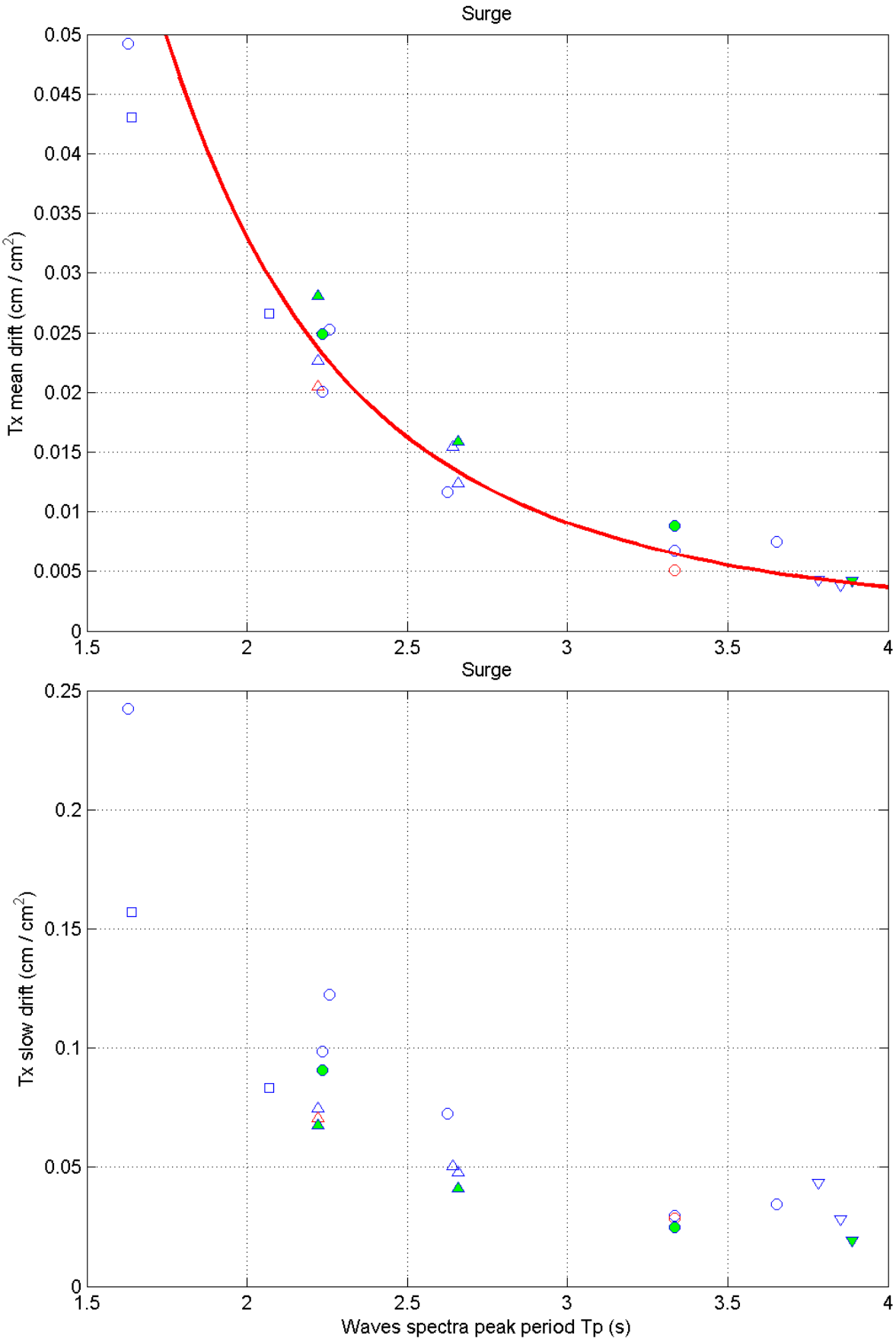

Figure 3.4 Irregular waves : mean surge drift and low frequency significant surge.

4 CONCLUSIONS AND RECOMMENDATIONS

4.1 EVALUATION OF THE LOW FREQUENCY EFFECTS

Approach based on a perfect fluid assumption for the wave loads on a moored buoy show enough accuracy to evaluate the mean drift effects. However additional damping is required to calibrate the resonant phenomenon at first order in heave and pitch motion that influence the second order surge drift.
Obviously, numerical results show that the influence of a power take off unit on drift motion can be important. This should be illustrated by a documented case study with experimental results.

4.2 MOORING LINES EFFECTS

The natural periods of the horizontal motions depends on the mooring stiffness and on the floating body inertia.
In the case study considered here, these natural periods are long and lead to both waves frequency and low frequency responses.
The effects of the mooring lines on the low frequency behaviour of the buoy is twofold.
First, the diameter of the line may influence the mean surge drift, a larger diameter increases the mean surge motion.
Second, the mooring line diameter may influence the slow drift motions, a larger diameter with roughness decreases the low frequency amplitude.
The mooring lines damping can be approximated by semi analytical formulas in the case of quasi-static behaviour (see appendices).
Complementary tests and analysis should be conducted with forced top motions on the mooring lines in order to identify the inertia and damping effects in different configurations: wave frequency motion only, low frequency motion only, combined wave and low frequency motions, and compare the experimental damping to the numerical approximation.
Additional work should be done to evaluate the slow drift surge motion from the Quadratic Transfer Function and the numerical low frequency damping and compare it to the experimental results.

5 REFERENCES

X. Bompais, M. Le Boulluec, F. Dekindt, S. Marin, B. Molin . "Slow- Drift Motion : Practical Estimation of Mooring Line Damping". Proc. 13th OMAE Conference, 1994, Houston

X.B. Chen. "Hydrodynamics in Offshore and Naval Applications – Part I." . Keynote lecture at the 6th Intl Conf HydroDynamics, November, 2004. Perth (Australia).

Chen, XB., Rezende, F., 2009, "Efficient computations of second-order low-frequency wave load". *Proceedings 28th International Conference on Offshore Mechanics and Arctic Engineering (OMAE2009)*, paper OMAE2009-79522, ASME, New York, USA.

J Jamsek, A Stefanovska, P.V. E. McClintock, and I.A. Khovanov. Time-phase bispectral analysis. Physical Review E 68, 016201, 2003

N. Kim. Extraction Of The Second-Order Nonlinear Response From Model Test Data In Random Seas And Comparison Of The Gaussian And Non-Gaussian Models. Dissertation Submitted to the Office of Graduate Studies of Texas A&M University. December 2004

M. Le Boulluec, P. Le Buhan, X.B. Chen, G. Deleuil, L. Foulhoux, B. Molin, F. Villeger. "Recent Advances on the Slow-Drift Damping of Offshore Structures". Proc. of the 7th Int. Conf. on the Behaviour of Offshore Structures, BOSS'94, july 1994, Pergamon, Vol 2, pp 9-30.

Ch. Lee, JN. Newman, MH. Kim, DKP Yue. The computation of second-order wave loads by WAMIT. Proc OMAE Stavanger, Norway 1991; 113–23.

Ch. Retzler, Ocean Power Delivery Ltd, Edinburgh, UK. Measurements of the slow drift dynamics of a model Pelamis wave energy converter. Renewable Energy 31 (2006) 257–269

A. Sarkar and R. Eatock Taylor. Low-frequency responses of non-linearly moored vessels in random waves: development of a two-scale perturbation method. Applied Ocean Research, Volume 20, Issue 4, August 1998, Pages 225-236

A. Sarkar and R. Eatock Taylor. Effects of mooring line drag damping on response statistics of vessels excited by first- and second-order wave forces. Ocean Engineering, Volume 27, Issue 6, June 2000, Pages 667-686

A. Sarkar and R. Eatock Taylor. Low-frequency responses of non-linearly moored vessels in random waves: coupled surge, pitch and heave motions. Journal of Fluids and Structures, Volume 15, Issue 1, January 2001, Pages 133-150

I. A. Sibetheros, O. R. Rijken and J. M. Niedzwecki. Volterra series-based system analysis of random wave interaction with a horizontal cylinder. Ocean Engineering, Volume 27, Issue 3, March 2000, Pages 241-270

S. Weller, P. Davies, L. Johanning.The Influence of Load History on Synthetic Rope Response Proc EWTEC Aalborg, Septembre 2013

6 APPENDICES

Semi analytical methods to evaluate the influence of the moorings on the slow drift damping.

Low frequency response on multi-chromatic waves

Bi-chromatice waves:

First order input → Linear + Quadratic transfer → First + second order response

$\omega_1 \quad \omega_2$
$a_1 \quad a_2$

Waves frequencies	$\omega_1 \quad a_1$	$\omega_2 \quad a_2$
Low frequencies	$\omega_2 - \omega_1$	$a_1 a_2$
Mean drift	0	$a_1^2 \quad a_2^2$
High frequencies	$\omega_1 + \omega_2$	$a_1 a_2$
	$2\omega_1$	a_1^2
	$2\omega_2$	a_2^2

Multi-chromatic waves:

First order input → Linear + Quadratic transfer → First + second order response

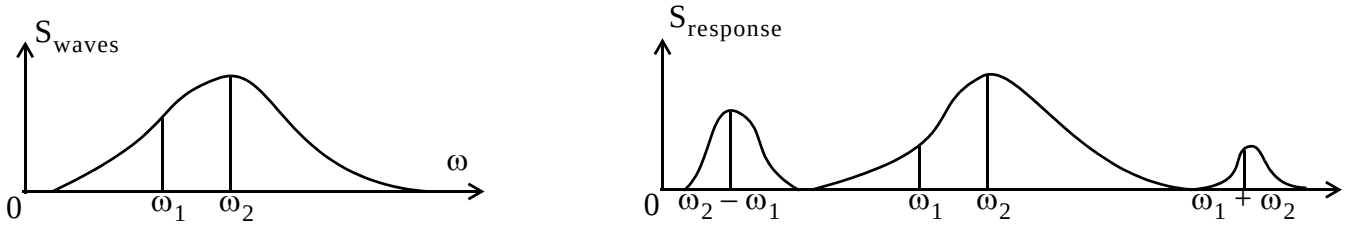

Low frequency dynamics:

$$(M + M_{a\infty})\ddot{X} + B\dot{X} + KX = F_{lf}$$

$$F_{lf} = [a_j e^{i(\omega_j t + \varphi_j)}][QTF_{jk}][a_k e^{-i(\omega_k t + \varphi_k)}]$$

Quadratic Transfer Function (hermitian matrix):

$$\begin{array}{c} \\ \omega_j \end{array} \overset{\omega_k}{\begin{bmatrix} QTF_{11} & QTF_{12} & \dots & QTF_{1k} & \dots & QTF_{1,n-1} & QTF_{1n} \\ QTF_{21} & QTF_{22} & \dots & QTF_{2k} & \dots & QTF_{2,n-1} & QTF_{2n} \\ \dots & \dots & \dots & \dots & \dots & \dots & \dots \\ QTF_{j1} & QTF_{j2} & \dots & QTF_{jk} & \dots & QTF_{j,n-1} & QTF_{jn} \\ \dots & \dots & \dots & \dots & \dots & \dots & \dots \\ QTF_{n-1,1} & QTF_{n-1,2} & \dots & \dots & \dots & QTF_{n-1,n-1} & QTF_{n-1,n} \\ QTF_{n1} & QTF_{n2} & \dots & QTF_{nk} & \dots & QTF_{n,n-1} & QTF_{nn} \end{bmatrix}} \qquad |\omega_j - \omega_k| = \Omega$$

Diagonal = mean drift force F_d.

Low frequency force spectrum:

$$S_{FF}(\Omega) = 8\int_0^\infty S(\omega)S(\omega+\Omega)\left|F_{lf}(\omega,\omega+\Omega)\right|^2 d\omega$$

Approximation:

$$F_{lf}(\omega_1,\omega_2) = \sqrt{\left|F_d(\omega_1)F_d(\omega_2)\right|}\,\mathrm{sgn}(F_d) \qquad S_{FF}(\Omega) = 8\int_0^\infty S(\omega)S(\omega+\Omega)F_d(\omega)F_d(\omega+\Omega)d\omega$$

Low frequency motion spectrum:

$$S_{XX}(\Omega) = \frac{S_{FF}(\Omega)}{[K-(M+M_a)\Omega^2]^2 + B^2\Omega^2}$$

For a narrow banded spectrum around the natural frequency:

$$\sigma^2 = \int_0^\infty \frac{S_{FF}(\Omega)}{[K-(M+M_a)\Omega^2]^2 + B^2\Omega^2}d\Omega = \frac{S_{FF}(\Omega_o)}{(M+M_a)^2}\int_{\substack{\Omega_o-\varepsilon\Omega_o \\ \varepsilon\to 0}}^{\Omega_o+\varepsilon\Omega_o} \frac{d\Omega}{[\Omega_o^2-\Omega^2]^2 + 4\alpha^2\Omega_o^2\Omega^2} \qquad \alpha = \frac{B}{B_c}$$

The spectrum variance is inversely proportional to the low frequency damping: $\sigma^2 = \dfrac{\pi S_{FF}(\Omega_o)}{2BK}$

Wave drift damping

For surge motion:

$$F_{dX}(\omega, \dot{X}) = F_{dX}(\omega, 0) + \frac{\partial}{\partial V_{xa}} F_{dX}(\omega, V_{xa})\Big|_{V_{xa}=0} \dot{X} \qquad B_{dXX}(\omega) = \frac{\partial}{\partial V_a} F_{dX}(\omega, V_{xa})\Big|_{V_{xa}=0}$$

For a wave spectrum::

$$B_d = 2\int_0^\infty S(\omega) B_{dXX}(\omega) d\omega$$

Two methods for wave drift damping computation :

- direct method: $B_{dXX}(\omega, V) = \frac{F_{dX}(\omega, V + \delta V) - F_{dX}(\omega, V - \delta V)}{2\delta V}$

- corrected gradient heuristic method:

$$B_{dXX}(\omega, 0) = \frac{\omega^2}{g} \frac{\partial}{\partial \omega} F_{dX}(\omega, 0) + 4\frac{\omega}{g} F_{dX}(\omega, 0$$

Viscous damping

Morison force on a slender body (line):

Relative velocity: $\vec{V}_r = \vec{V}_{fluid} - \vec{V}_{line}$

Normal relative velocity: $\vec{V}_{rn} = \vec{V}_{fn} - \vec{V}_{ln}$

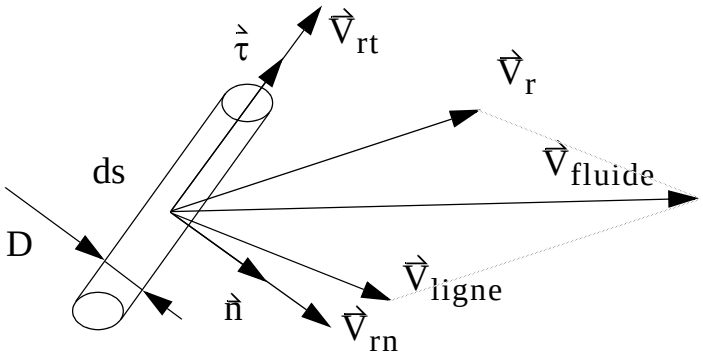

$$\frac{d\vec{F}}{ds} = \rho\frac{\pi D^2}{4}\left[(1 + C_m)\frac{d\vec{V}_{fn}}{dt} - C_m\frac{d\vec{V}_{ln}}{dt}\right]$$

Inertia component

$$+ \frac{1}{2}\rho D C_N \left\|\vec{V}_{rn}\right\| \vec{V}_{rn}$$

Drag component

Simplified case, no incident flow:

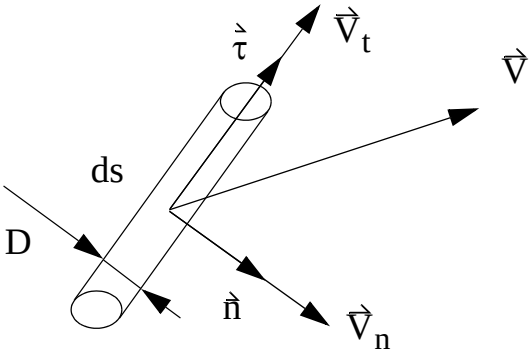

$$\vec{V} = \vec{V}_{line}$$

$$\vec{V}_t = (\vec{V} \cdot \vec{\tau})\vec{\tau}$$

$$\vec{V}_n = \vec{V} - (\vec{V} \cdot \vec{\tau})\vec{\tau}$$

$$\vec{n} = \frac{\vec{V} - (\vec{V} \cdot \vec{\tau})\vec{\tau}}{\left\|\vec{V} - (\vec{V} \cdot \vec{\tau})\vec{\tau}\right\|}$$

$$\frac{d\vec{F}}{ds} = -\rho\frac{\pi D^2}{4} C_m \frac{d\vec{V}_n}{dt} - \frac{1}{2}\rho D C_N \left\|\vec{V}_n\right\| \vec{V}_n$$

Purely transverse drag force in bi-chromatic case:

$v = \omega a \cos\omega t$

$V = \Omega A \cos\Omega t \qquad v \gg V$

$\omega, \Omega, a, A > 0$

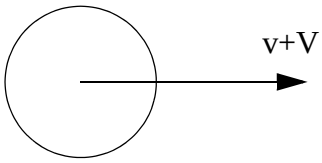

$$\gamma = \frac{1}{2}\rho d D C_N$$

Harmonics of the drag force in bi-chromatic case::

$$F_d = -\gamma(v+V)|v+V| \qquad |v+V|(v+V) = v|v| + 2|v|V + \mathrm{sgn}\, v V^2$$

$$\mathrm{sgn}(\cos\omega t) = \sum_{k=0}^{\infty} \frac{4(-1)^k}{(2k+1)\pi}\cos(2k+1)\omega t = \frac{4}{\pi}\left(\cos\omega t - \frac{1}{3}\cos 3\omega t + \ldots\right)$$

$$|v| = v\,\mathrm{sgn}\, v = \frac{2}{\pi}\omega a\left(1 + \frac{2}{3}\cos 2\omega t + \ldots\right)$$

$$F_d = -\gamma v|v| - \frac{4}{\pi}\gamma\omega a V - \ldots$$

Energy considerations:

Two basic kind of forces :

- linear force: $F = -\Lambda V$
- quadratic force (drag): $F = -\gamma V|V|$

Power dissipation by a linear force:

$$V = V_m \cos\Omega t \qquad F = -\Lambda V \qquad P = FV = -\Lambda V^2 \qquad \bar{P} = \frac{1}{T}\int_0^T P dt = -\frac{\Lambda}{2} V_m{}^2$$

Power dissipation by a qudratic force with low frequency velocity:

$$V = V_m \cos\Omega t \qquad F = -\gamma V|V| \qquad P = FV = -\gamma V^3 \qquad \bar{P} = \frac{1}{T}\int_0^T P dt = -\frac{4}{3\pi}\gamma V_m{}^3$$

$$\gamma = \frac{1}{2}\rho L D C_N \qquad F = -\gamma V|V| \approx -\frac{4}{3\pi}\rho L D C_N V_m V$$

The equivalent linear damping is proportional to the low frequency velocity.

Power dissipation by a quadratic force with bi-chromatic velocity:

$V = V_m \cos\Omega t$ $\qquad F = -\gamma(v+V)|v+V| \approx -\gamma(v|v| + 2|v|V + \mathrm{sgn}\, v V^2)$

$v = v_m \cos\omega t$ $\qquad P = FV \approx -\gamma(v|v| + 2|v|V + \mathrm{sgn}\, v V^2)V$

$v \gg V$

$$P_{LF} \approx -2\gamma|v|V^2 \qquad \overline{P_{LF}} = -2\frac{2}{\pi}\gamma v_m \frac{1}{2} V_m{}^2 \qquad F_{LF} \approx -\frac{2}{\pi}\rho L D C_N v_m V$$

$$\gamma = \frac{1}{2}\rho L D C_N \qquad \Lambda \approx \frac{4}{\pi}\gamma v_m = \frac{2}{\pi}\rho L D C_N v_m$$

The equivalent linear damping is proportional to the wave frequency velocity.

Damping induced by a catenary mooring line:

Moored system

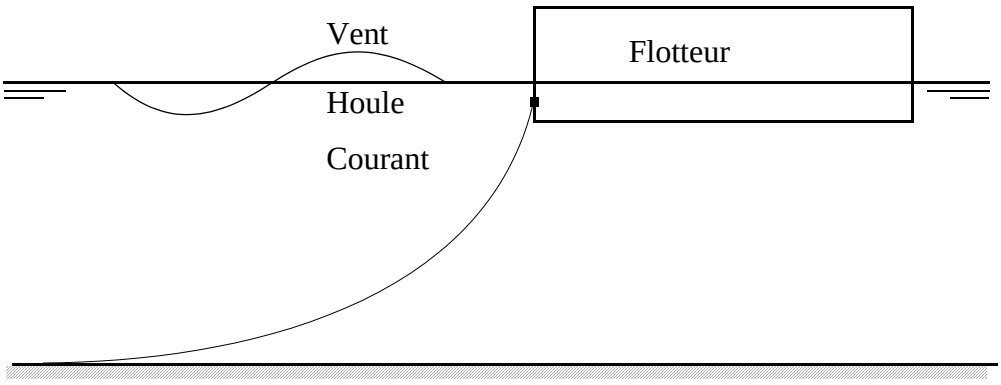

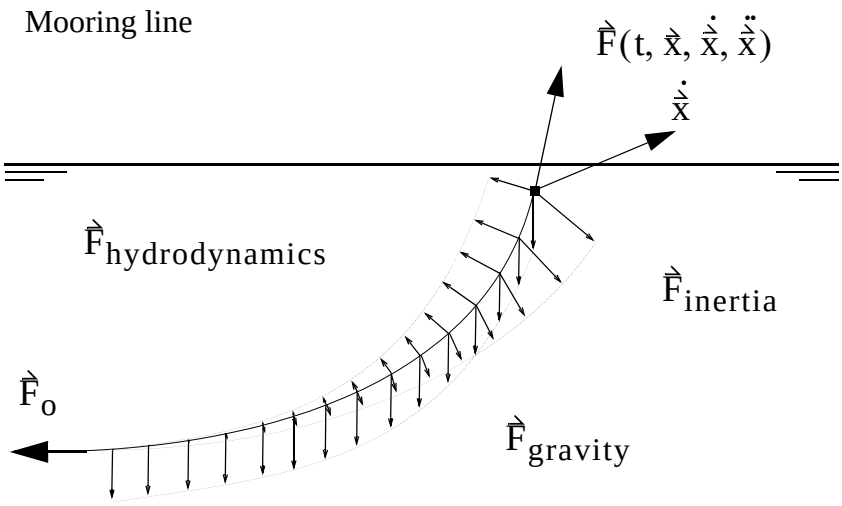

$$\vec{F}(t, \vec{x}, \dot{\vec{x}}, \ddot{\vec{x}}) = \vec{F}_{stiffness}(t, \vec{x}) + \vec{F}_{inertia}(t, \ddot{\vec{x}}) + \vec{F}_{damping}(t, \dot{\vec{x}})$$

Energy dissipation is calculated with consideration of a quasi-static motion of the mooring line.

Velocity along the mooring line:

τ is the tangent vector, the normal V_n et tangential V_t components of the velocity V are:

$$\vec{V}_t = (\vec{V} \cdot \vec{\tau})\vec{\tau} \qquad \vec{V}_n = \vec{V} - (\vec{V} \cdot \vec{\tau})\vec{\tau} \qquad \vec{n}_{hydro} = \frac{\vec{V} - (\vec{V} \cdot \vec{\tau})\vec{\tau}}{\left\| \vec{V} - (\vec{V} \cdot \vec{\tau})\vec{\tau} \right\|}$$

Motions of a point a(dx_a, dy_a, dz_a) located on the ligne are related to the motions at the top end of the line e(dx_e, dy_e, dz_e):

$$\begin{bmatrix} dx_a \\ dy_a \\ dz_a \end{bmatrix} = \begin{bmatrix} \alpha_{xx} & 0 & \alpha_{xz} \\ 0 & \alpha_{yy} & 0 \\ \alpha_{zx} & 0 & \alpha_{zz} \end{bmatrix} \begin{bmatrix} dx_e \\ dy_e \\ dz_e \end{bmatrix} \qquad \begin{bmatrix} V_{xa} \\ V_{ya} \\ V_{za} \end{bmatrix} = \begin{bmatrix} \alpha_{xx} & 0 & \alpha_{xz} \\ 0 & \alpha_{yy} & 0 \\ \alpha_{zx} & 0 & \alpha_{zz} \end{bmatrix} \begin{bmatrix} V_{xe} \\ V_{ye} \\ V_{ze} \end{bmatrix}$$

Matrix coefficients α can be expressed with the parameters of the catenary shape.

n_o is the normal vector into the catenary line plane at rest.

$$\vec{V}_t = (\vec{V}\cdot\vec{\tau})\vec{\tau} = (V_{xa}n_{oz} - V_{za}n_{ox})\vec{\tau} \qquad \|\vec{V}_t\| = |V_{xa}n_{oz} - V_{za}n_{ox}| \qquad \vec{n} = \frac{(\vec{V}\cdot\vec{n}_o)\vec{n}_o + V_{ya}\vec{j}}{\sqrt{(\vec{V}\cdot\vec{n}_o)^2 + V_{ya}^2}}$$

$$\vec{V}_n = \vec{V} - (\vec{V}\cdot\vec{\tau})\vec{\tau} = (\vec{V}\cdot\vec{n}_o)\vec{n}_o + V_{ya}\vec{j}$$

$$V_n^2 = (V_{xa}n_{ox} + V_{za}n_{oz})^2 + V_{ya}^2 = (\vec{V}\cdot\vec{n}_o)^2 + V_{ya}^2$$

$$V_{ya} = 0 \Rightarrow \|\vec{V}_n\| = |V_{xa}n_{ox} + V_{za}n_{oz}| = |\vec{V}\cdot\vec{n}_o| \qquad V_{ya} = 0 \Rightarrow \vec{n} = \vec{n}_o \qquad \vec{\tau} = \vec{n}_o \wedge \vec{j}$$

$$\vec{V}_n = \begin{bmatrix} \beta_x n_{ox} & 0 & \beta_z n_{ox} \\ 0 & \beta_y & 0 \\ \beta_x n_{oz} & 0 & \beta_z n_{oz} \end{bmatrix} \begin{bmatrix} V_{xe} \\ V_{ye} \\ V_{ze} \end{bmatrix} \qquad \begin{aligned} \beta_x &= \alpha_{xx}n_{ox} + \alpha_{zx}n_{oz} \\ \beta_y &= \alpha_{yy} \\ \beta_z &= \alpha_{xz}n_{ox} + \alpha_{zz}n_{oz} \end{aligned} \qquad V_n^2 = [\beta_x V_{xe} + \beta_z V_{ze}]^2 + \beta_y^2 V_{ye}^2$$

Monochromatic case:

Energy dissipation: $\int_T (B\vec{V}_e)\cdot\vec{V}_e dt = \iint_{TL} \frac{1}{2}\rho D C_n \|\vec{V}_n\|^3 ds dt$

where: $\|\vec{V}_n\|^3 = \|\vec{V}_n\|\|\vec{V}_n\|^2 = \|\vec{V}_n\|(\beta_x^2 V_{ex}^2 + \beta_z^2 V_{ez}^2 + \beta_y^2 V_{ey}^2 + 2\beta_z\beta_x V_{ez}V_{ex})$

Equivalence with a linear equivalent damping gives:

$$\int_T [B_{xx}V_{ex}^2 + B_{yy}V_{ey}^2 + B_{zz}V_{ez}^2 + (B_{xy}+B_{yx})V_{ex}V_{ey} + (B_{yz}+B_{zy})V_{ey}V_{ez} + (B_{zx}+B_{xz})V_{ez}V_{ex}]dt$$
$$= \iint_{TL} \frac{1}{2}\rho D C_n \|\vec{V}_n\|(\beta_x^2 V_{ex}^2 + \beta_z^2 V_{ez}^2 + \beta_y^2 V_{ey}^2 + 2\beta_z\beta_x V_{ez}V_{ex})ds dt$$

Une approximation des coefficients de la matrice d'amortissement équivalente est donc la suivante :

$$B_{xx} = \int_L \rho D C_n \frac{4}{3\pi}\|\vec{V}_{nm}\|\beta_x^2 ds \qquad B_{yy} = \int_L \rho D C_n \frac{4}{3\pi}\|\vec{V}_{nm}\|\beta_y^2 ds \qquad B_{zz} = \int_L \rho D C_n \frac{4}{3\pi}\|\vec{V}_{nm}\|\beta_z^2 ds$$

$$B_{xy} = 0 \qquad B_{yz} = 0 \qquad B_{zx} = \int_L \rho D C_n \frac{4}{3\pi}\|\vec{V}_{nm}\|\beta_z\beta_x ds$$

The equivalent damping is of quadratic form.

Bi-chromatic case:

The velocity is composed of a low frequency component (LF) and a wave (high) frequency component (HF).

Energy dissipation: $\int_T (B\vec{V}_{LFe}) \cdot \vec{V}_{LFe} dt = \int\int_{TL} \frac{1}{2}\rho DC_n \left\|\vec{V}_n\right\| (\vec{V}_n \cdot \overrightarrow{V_{LF}}) ds dt$

where:

$$\left\|\vec{V}_n\right\| \vec{V}_n \cdot \vec{V}_{LF} = \left\|\vec{V}_{LFn} + \vec{V}_{HFn}\right\| (\vec{V}_{LFn} + \vec{V}_{HFn}) \cdot \vec{V}_{LFn}$$
$$= \left\|\vec{V}_{LFn} + \vec{V}_{HFn}\right\| \left\|\vec{V}_{LFn}\right\|^2 + \left\|\vec{V}_{Ln} + \vec{V}_{HFn}\right\| (\vec{V}_{HFn} \cdot \vec{V}_{LFn})$$

$$\left\|\vec{V}_{LFn} + \vec{V}_{HFn}\right\| \left\|\vec{V}_{LFn}\right\|^2 + \left\|\vec{V}_{LFn} + \vec{V}_{HFn}\right\| (\vec{V}_{HFn} \cdot \vec{V}_{LFn}) =$$
$$\left\|\vec{V}_{HFn}\right\| (\vec{V}_{HFn} \cdot \vec{V}_{LFn}) + \left\|\vec{V}_{HFn}\right\| \left\|\vec{V}_{LFn}\right\|^2 + \frac{(\vec{V}_{HFn} \cdot \vec{V}_{LFn})^2}{\left\|\vec{V}_{HFn}\right\|} + o\left(\frac{\left\|\vec{V}_{LFn}\right\|^2}{\left\|\vec{V}_{HFn}\right\|^2}\right)$$

.

$$\left\|\vec{V}_{HFn}\right\| \left\|\vec{V}_{LFn}\right\|^2 = \sqrt{[\beta_x V_{HFxe} + \beta_z V_{HFze}]^2 + \beta_y^2 V_{HFye}^2} \times ([\beta_x V_{LFxe} + \beta_z V_{LFze}]^2 + \beta_y^2 V_{LFye}^2)$$
$$\frac{(\vec{V}_{HFn} \cdot \vec{V}_{LFn})^2}{\left\|\vec{V}_{HFn}\right\|} = \frac{([\beta_x V_{HFxe} + \beta_z V_{HFze}][\beta_x V_{LFxe} + \beta_z V_{LFze}] + \beta_y^2 V_{HFye} V_{LFye})^2}{\sqrt{[\beta_x V_{HFxe} + \beta_z V_{HFze}]^2 + \beta_y^2 V_{HFye}^2}}$$

Then:

$$B_{xx} = \frac{1}{T}\int\int_{LT} \rho DC_n \frac{([\beta_x V_{HFxe} + \beta_z V_{HFze}]^2 + \beta_y^2 V_{HFye}^2/2)}{\sqrt{[\beta_x V_{HFxe} + \beta_z V_{HFze}]^2 + \beta_y^2 V_{HFye}^2}} \beta_x^2 ds$$
$$B_{yy} = \frac{1}{T}\int\int_{LT} \rho DC_n \frac{([\beta_x V_{HFxe} + \beta_z V_{HFze}]^2/2 + \beta_y^2 V_{HFye}^2)}{\sqrt{[\beta_x V_{HFxe} + \beta_z V_{HFze}]^2 + \beta_y^2 V_{HFye}^2}} \beta_y^2 ds$$
$$B_{zz} = \frac{1}{T}\int\int_{LT} \rho DC_n \frac{([\beta_x V_{HFxe} + \beta_z V_{HFze}]^2 + \beta_y^2 V_{HFye}^2/2)}{\sqrt{[\beta_x V_{HFxe} + \beta_z V_{HFze}]^2 + \beta_y^2 V_{HFye}^2}} \beta_z^2 ds$$
$$B_{xy} = \frac{1}{T}\int\int_{LT} \rho DC_n \frac{(\beta_x V_{HFxe} + \beta_z V_{HFze})(\beta_y V_{HFye})/2}{\sqrt{[\beta_x V_{HFxe} + \beta_z V_{HFze}]^2 + \beta_y^2 V_{HFye}^2}} \beta_x \beta_y ds$$
$$B_{yz} = \frac{1}{T}\int\int_{LT} \rho DC_n \frac{(\beta_x V_{HFxe} + \beta_z V_{HFze})(\beta_y V_{HFye})/2}{\sqrt{[\beta_x V_{HFxe} + \beta_z V_{HFze}]^2 + \beta_y^2 V_{HFye}^2}} \beta_y \beta_z ds$$
$$B_{zx} = \frac{1}{T}\int\int_{LT} \rho DC_n \frac{([\beta_x V_{HFxe} + \beta_z V_{HFze}]^2 + \beta_y^2 V_{HFye}^2/2)}{\sqrt{[\beta_x V_{HFxe} + \beta_z V_{HFze}]^2 + \beta_y^2 V_{HFye}^2}} \beta_z \beta_x ds$$

The equivalent linear damping depends on the waves frequency velocity of the mooring line.

Quasi static deformation of a catenary line

In the equilibrium plane:

O : origin
x : horizontal
z : vertical
y : perpendicular

l : length
h : vertical distance
d : horizontal distance
x_o : abscissa of the minimum point
z_o : altitude of the minimum point

a : current point
e : top end point

T : total tension
T_x : horizontal tension (constant value= T_o)
T_z : vertical tension
ϖ : distributed weight

Θ : angle
τ_x : horizontal component of the tanget vector
τ_z : vertical component of the tangent vector

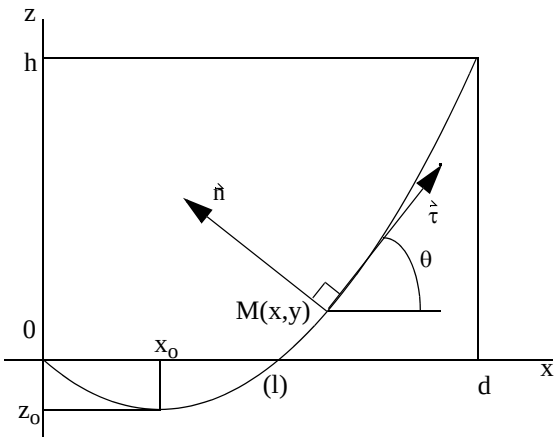

$$ds = \sqrt{(dx)^2 + (dz)^2} \qquad \frac{dz}{dx} = \frac{T_z}{T_x} = \tan\theta$$

Equilibrium: $dT_x = 0 \Rightarrow T_x = T_o = C_{te}$

$$dT_z = \varpi ds \Rightarrow dT_z = \varpi\sqrt{1 + \left(\frac{dz}{dx}\right)^2}\,dx$$

$$\frac{d\left(\frac{T_z}{T_o}\right)}{\sqrt{1 + \left(\frac{dz}{dx}\right)^2}} = \frac{\varpi dx}{T_o} \Rightarrow \operatorname{asinh}\frac{T_z}{T_o} = \frac{\varpi(x - x_o)}{T_o}$$

$$\frac{dz}{dx} = \sinh\frac{\varpi(x - x_o)}{T_o}$$

$$z - z_o = \frac{T_o}{\varpi}\cosh\frac{\varpi(x - x_o)}{T_o} - 1$$

Non dimensionnel parameters:

$$L = \frac{\varpi l}{T_o} \quad D = \frac{\varpi d}{T_o} \quad H = \frac{\varpi h}{T_o} \quad S = \frac{\varpi s}{T_o} \quad X = \frac{\varpi x}{T_o} \quad Y = \frac{\varpi y}{T_o} \quad Z = \frac{\varpi z}{T_o}$$

Geometry, internal tension:

$$Z_a = Z_o + \cosh(X_a - X_o) - 1 \qquad \tau_x = \frac{1}{\cosh(X_a - X_o)} \qquad \tau_z = \tanh(X_a - X_o) \qquad \tan\theta_a = \sinh(X_a - X_o)$$

$$S_a = S_o + \sinh(X_a - X_o) \qquad T_x = T_o \qquad T_z = T_o \sinh(X_a - X_o) \qquad T = T_o \cosh(X_a - X_o)$$

Low point is fixed:

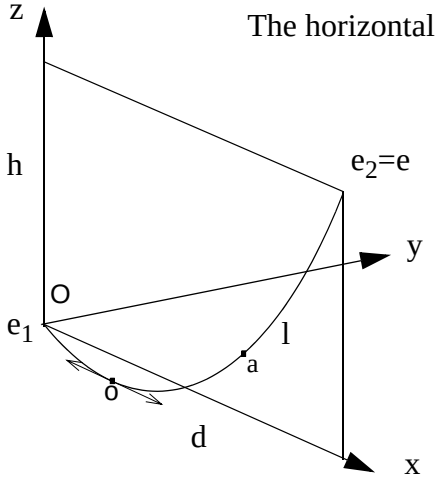

The horizontal tension T_o is related to ξ_o solution of equation :

$$\sinh\xi = a\xi \qquad \xi = \frac{D}{2} \qquad a = \frac{\sqrt{l^2 - h^2}}{d} = \frac{\sqrt{L^2 - H^2}}{D}$$

Quasi-static displacement of a point of the line:

$$T_d = \frac{\sinh D}{D\sinh D + H^2 - L^2} \qquad T_h = \frac{H}{D\sinh D + H^2 - L^2}$$

$$X_d = \frac{-(L^2 - H^2)}{2(D\sinh D + H^2 - L^2)} \qquad X_h = \frac{-DH}{2(D\sinh D + H^2 - L^2)} - \frac{L}{L^2 - H^2}$$

$$dx_a = (1 - \tau_x \cosh X_o)(X_d dx_e + X_h dz_e) + (X_a - \tau_x S_a)(T_d dx_e + T_h dz_e)$$

$$dy_a = \frac{Y_a}{D} dy_e$$

$$dz_a = -(\sinh X_o + \tau_z \cosh X_o)(X_d dx_e + X_h dz_e) + (Z_a - \tau_z S_a)(T_d dx_e + T_h dz_e)$$

Stiffness matrix :

$$\begin{bmatrix} dT_{xe} \\ dT_{ye} \\ dT_{ze} \end{bmatrix} = \frac{\varpi}{D\sinh D + H^2 - L^2} \begin{bmatrix} \sinh D & 0 & H \\ 0 & 0 & 0 \\ H & 0 & \dfrac{\sinh D(D\sinh D + H^2 - L^2) + H^2 D}{L^2 - H^2} \end{bmatrix} \begin{bmatrix} dx_e \\ dy_e \\ dz_e \end{bmatrix}$$

Low point is the touch down point:

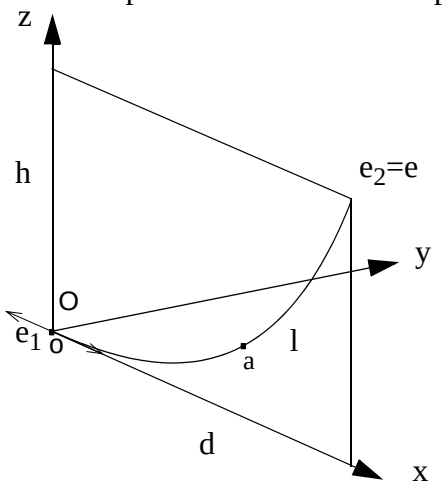

$$T_o = T_2 - \varpi h \qquad T_1 = T_o \qquad L^2 = H^2 + 2H$$

$$T_{z2} = \varpi l \qquad D = \operatorname{asinh} L$$

Stiffness matrix:

$$\begin{bmatrix} dT_{xe} \\ dT_{ye} \\ dT_{ze} \end{bmatrix} = \frac{\varpi}{LD - 2H} \begin{bmatrix} L & 0 & H \\ 0 & 0 & 0 \\ H & 0 & D(H+1) - L \end{bmatrix} \begin{bmatrix} dx_e \\ dy_e \\ dz_e \end{bmatrix}$$

Quasi-static displacement of a point of the line:

$$dx_a = \frac{1}{LD - 2H}[[L(X_a - \tau_x S_a) + H(\tau_x - 1)]dx_e + [H(X_a - \tau_x S_a) + [D(H+1) - L](\tau_x - 1)]dz_e]$$

$$dy_a = \frac{Y_a}{D} dy_e$$

$$dz_a = \frac{1}{LD - 2H}[[L(Z_a - \tau_z S_a) + H\tau_z]dx_e + [H(Z_a - \tau_z S_a) + [D(H+1) - L]\tau_z]dz_e]$$